Available online at www.sciencedirect.com
SCIENCE DIRECT®
International Journal of Mass Spectrometry 241 (2005) 283–294
International Journal of Mass Spectrometry
www.elsevier.com/locate/ijms

A theoretical study of trivalent lanthanide ion microsolvation in water clusters from first principles

Sean R. Hughes, Tao-Nhân Nguyen, John A. Capobianco, Gilles H. Peslherbe*

Centre for Research in Molecular Modeling (CERMM), Department of Chemistry and Biochemistry, Concordia University, 7141 Sherbrooke St. West, Montréal, Que., Canada H4B 1R6

Received 2 December 2004; accepted 15 December 2004

Dedicated to Bill Hase on the occasion of his 60th birthday.

Abstract

Although metal ion–water clusters $M^{m+}(H_2O)_n$ have been widely studied for many singly charged metal ions, thermodynamic and structural studies of di- or trivalent metal ion–water clusters remain relatively rare. We have investigated the structural and thermodynamic properties of $Ln^{3+}(H_2O)_n$ clusters ($Ln^{3+} = Nd^{3+}$, Eu^{3+}, Er^{3+} and Yb^{3+}) by means of Monte Carlo simulations using newly-developed, polarizable model potentials parameterized on the basis of ab initio calculations for small clusters. We report total cluster enthalpies and stepwise cluster binding enthalpies predicted by our simulations. Our results also indicate that Ln^{3+} ions exhibit a well-defined interior solvation shell structure. At small cluster sizes ($n = 6$–12), the first-shell coordination numbers are close to 6 or 7, whereas convergence towards bulk-like coordination numbers seems to be achieved at cluster size $n \geq 24$. In contrast, convergence of the thermodynamic properties towards bulk values only occurs at much larger cluster sizes, $n \geq 64$.

Keywords: Cluster ions; Lanthanide; Model potentials; Coordination structure; Thermodynamics; Monte Carlo simulations

1. Introduction

The microsolvation of metal ions in the gas phase has been the focus of intensive research over the last 20 years [1–4]. Particular attention has been paid to the energetic, structural and spectroscopic properties of ionic clusters containing monovalent metal ions. However, despite advanced techniques that allow for the generation of multiply charged, solvated metal ion clusters [5–18], they have not been studied extensively, especially those clusters containing trivalent metal ions [9–15]. Understanding the fundamental interactions involved in the formation of these clusters, such as the metal-to-ligand bond, can yield insight into the properties of larger clusters or even bulk solutions [19,20]. One of the most pertinent solvents is obviously water, which is ubiquitous in chemistry and biology.

In an effort to probe the interactions between trivalent metal ions and water, we have opted to investigate $Ln^{3+}(H_2O)_n$ clusters, paying particular attention to their structural and thermodynamic properties. The lanthanides are particularly interesting due to their rather unique binding properties, which contrast with their transition metal counterparts [21]. Despite large, ion-ligand binding energies [5,22–27], the lanthanide ions are believed to form predominantly ionic complexes with their ligands. This is owed to the shielding of the 4f-orbitals by the outermost 5p and 5s electrons, which prevents them from participating in metal to ligand covalent binding [21]. In addition, these ions exhibit a flexible coordination chemistry, binding anywhere from 6 to 10 ligands. Even though the preferential coordination numbers of lanthanide ions in solution had

* Corresponding author. Tel.: +1 514 848 2424x3335; fax: +1 514 848 2868.
E-mail address: ghp@alcor.concordia.ca (G.H. Peslherbe).

1387-3806/$ – see front matter © 2004 Elsevier B.V. All rights reserved.
doi:10.1016/j.ijms.2004.12.023

been the subject of a heated debate in the past, it is now widely accepted that the coordination numbers are closer to nine for the lighter lanthanide ions and eight for the heavier ions. This phenomenon is attributed to 'lanthanide contraction', or the reduction in ionic size across the lanthanide series [28–34]. Because of these features, lanthanide ions provide the foundation for many electro-luminescent devices [21].

Despite sustained efforts, there has been limited success in detecting trivalent lanthanide–solvent clusters with protic solvents, in particular with water as a solvent [8–11]. Trivalent lanthanide metals have been shown to be prone to dissociative electron or proton transfer, resulting in the production of either $M^{2+}X(HOR)_n$ or $M^{2+}OR(HOR)_n$ species [11], an observation that has yet to be explained, given that the third ionization potential of some lanthanide metals, such as La and Ce, is lower than the second ionization potential of Cu, which is known to form stable $Cu^{2+}(H_2O)_n$ clusters [11]. To date, only Shvartsburg has reported the successful retention of the 3+ state of lanthanide metals in clusters of a protic solvent, namely Ln^{3+}–diacetone alcohol clusters [11], and only for cluster sizes in the range of $n = 5$–8. On the other hand, it has been shown that the 3+ state can be readily conserved in clusters containing aprotic solvents such as acetonitrile, acetone, dimethyl formamide and dimethyl sulfoxide [8,9,12–15]. Shvartsburg has reported minimum lanthanide–solvent cluster sizes of $n = 1$–3 for acetonitrile [12] and $n = 2$–5 for dimethyl sulfoxide [13], while Walker et al. were able to detect stable Ho^{3+}–acetonitrile clusters, with the most stable cluster size determined to be $n = 6$ [8].

In the past, a variety of electrostatic potential models have been proposed to describe lanthanide ions in solution. Meier et al. proposed one of the earliest models [22], which was able to reproduce the experimental coordination number of La^{3+} in water, as reported by Habenschuss and Spedding [28]. However, this study failed to address other lanthanide ions and, thus, did not deal with the well known 'lanthanide shift' in coordination number [25,26]. Subsequent work by Helm and Merbach's groups [35–39], not only reproduced the observed trends in coordination across the series, but also determined the solvent exchange rates and coordination equilibria for Nd^{3+}, Sm^{3+} and Yb^{3+} in solution [38,39]. Furthermore, they were the first group to stress the importance of polarization for these systems, and they accounted for it by scaling the dipole moments of the solvent molecules in the first coordination shell. However, these models predicted bulk hydration enthalpies in poor agreement with experimental values [27,34]. More recent potentials for Ln^{3+} solutions proposed by Floris and Tani [25] yield structural results in good agreement with experiment, but fail to account for the appropriate coordination numbers of the late ions of the lanthanide series, namely Yb^{3+}. Finally, Derepas et al. [5] recently reported a model for $La^{3+}(H_2O)_n$ clusters up to size $n = 9$. Their findings indicated the preferential formation of 7 + 1 and 7 + 2 coordination structures as opposed to purely 8 or 9 coordinated species.

We have constructed a new, rigorous model potential, parameterized to reproduce properties of small ion–water clusters derived from quantum chemistry calculations. This is in contrast with the models presented earlier, which, with the exception of the work of Derepas et al. [5], were geared towards bulk, aqueous solvation. We have made use of our model potential to carry out room-temperature simulations of $Ln^{3+}(H_2O)_n$ clusters, specifically those involving Nd^{3+}, Eu^{3+}, Er^{3+}, and Yb^{3+}, in order to evaluate the structural and thermodynamic features of these clusters. These ions were chosen since they are characteristic of the trends in coordination across the series, in addition to their relevance as it relates to luminescence activity [21]. The outline of this article is as follows: we first discuss the results of quantum chemistry calculations for small $Ln^{3+}(H_2O)$ clusters. The latter serve as the basis for parameterization of our model potentials, which are presented in the following section along with the computational details of our simulations. The cluster structural features and thermodynamics resulting from our simulations are then presented and discussed. Concluding remarks follow immediately.

2. Quantum chemistry calculations for small $Ln^{3+}(H_2O)_n$ clusters

2.1. Computational details

Small, ground state $Ln^{3+}(H_2O)_n$ clusters were characterized by quantum chemistry calculations using the Gaussian 98 program [40]. Minimum energy structures were optimized without symmetry constraint using either the unrestricted Hartree-Fock (HF) method [41], Becke's three-parameter Lee-Yang-Parr (B3LYP) hybrid density functional theory [42,43] and second-order Møller-Plessett (MP2) perturbation theory [41]. Energies were also calculated with the Quadratic Configuration Interaction method [44] with single, double and linearized triple excitations [QCISD(T)] for MP2 optimized geometries. All minimum energy structures were characterized by a vibrational frequency analysis and the energies were corrected for both zero-point energy and basis-set superposition error via the Counterpoise approach [45]. The 6-31G+(2d,p) basis set was employed for water [46], as this basis set generates a rather accurate structure and a reasonable dipole moment for gas phase water at the MP2 level of theory. Approximate atomic charges and the resulting solvent dipole moments were evaluated with the electrostatic potential (ESP) method [47]. Lanthanide ions were represented by Stuttgart-Dresden-Bonn (SDD) large-core pseudopotentials and valence basis sets [48,49], which allow for an extensive description of the valence space and yields relatively accurate interaction energies [48,49].

Table 1
Structural, energetic and electronic properties of small $Ln^{3+}(H_2O)$ clusters[a]

Ion	Property	HF	B3LYP	MP2	QCISD(T)	Model[e]
Nd^{3+}	r_{Ln-O}[b]	2.32	2.29	2.30	2.30	2.36
	D_o[c]	85.5	98.0	87.3	88.7	88.7
	μ_{H_2O}[d]			3.27		6.03
Eu^{3+}	r_{Ln-O}[b]	2.27	2.24	2.26	2.26	2.34
	D_o[c]	90.5	103.7	92.3	94.3	92.7
	μ_{H_2O}[d]			3.37		6.17
Er^{3+}	r_{Ln-O}[b]	2.19	2.15	2.17	2.17	2.27
	D_o[c]	99.2	113.2	101.2	103.4	103.3
	μ_{H_2O}[d]			3.43		6.54
Yb^{3+}	r_{Ln-O}[b]	2.16	2.13	2.15	2.15	2.22
	D_o[c]	102.4	116.7	104.7	106.2	106.4
	μ_{H_2O}[d]			3.52		6.96

[a] Quantum chemistry calculations are performed with the 6-31+G(2d,p)/SDD basis set as discussed in the text.
[b] Lanthanide to oxygen distance (Å).
[c] Binding energy (kcal/mol) corrected for zero-point energy and basis set superposition error.
[d] Dipole moment (D) of water based on calculated, ESP charges [47].
[e] Prediction of model potentials.

2.2. $Ln^{3+}(H_2O)$ model—structural and energetic properties

Table 1 outlines the features of the minimum energy structures obtained from our quantum chemistry calculations for the $Ln^{3+}(H_2O)$ cluster model.[1]

All ion–water dimers possess C_{2v} symmetry. Most of the model chemistries yield similar binding energies and ion–water distances, and the latter agree well with those reported in the literature for bulk solutions [5,22–26]. Typically, the lanthanide ion will bind to oxygen at a distance of 2.30 Å in the case of Nd^{3+} and 2.15 Å for Yb^{3+} according to our MP2 calculations. As expected, the cluster binding energy is seen to increase across the series, from 88.7 kcal/mol for the Nd^{3+}–water dimer to 106.2 kcal/mol for the Yb^{3+}–water dimer according to our QCISD(T) calculations. The shifts in equilibrium ion–water distance are not surprising given that the heavier atoms possess an increased charge to size ratio and, thus, are more prone to inductive effects. Furthermore, the repulsive character of the interaction is reduced across the series due to the decrease in ionic size, leading to more favorable association between the ligand and ions. We note that the popular B3LYP method yields binding energies systematically overestimated by as much as 10 kcal/mol, compared to the more rigorous MP2 or QCISD(T) values. This is consistent with our previous findings for anionic clusters [50,51].

[1] We note that the deprotonated species $[Ln(OH)]^{2+}$ is predicted to be more stable than the $Ln^{3+}(H_2O)$ species by 40 kcal/mol, which may explain why small trivalent lanthanide–water clusters have not been observed experimentally, but these quantum chemistry calculations provide a basis for characterizing the interactions between water molecules and the trivalent ions in larger clusters.

Table 2
Changes in charge distributions and water structural properties in $Ln^{3+}(H_2O)$ clusters

Ion	Δq_{Ln}[a]	Δq_O[a]	Δq_H[a]	$\Delta\mu$[b]	Δr_{O-H}[c]	$\Delta\angle_{H-O-H}$[d]
Nd^{3+}	−0.15	−0.35	+0.25	1.16	0.03	−1.8
Eu^{3+}	−0.15	−0.39	+0.27	1.26	0.03	−1.7
Er^{3+}	−0.15	−0.44	+0.30	1.32	0.03	−1.5
Yb^{3+}	−0.16	−0.44	+0.30	1.41	0.03	−1.5

[a] Change in the atomic charge (e) upon complexation, based on calculated ESP charges [47].
[b] Change in the water dipole moment (D) upon complexation, based on calculated ESP charges [41]. The sum of the water atomic charges is not exactly zero, and the origin was chosen as the midpoint between the hydrogens in the calculation of the dipole moments.
[c] Change in water O–H distance (Å) upon complexation.
[d] Change in water angle (°) upon complexation.

2.3. $Ln^{3+}(H_2O)$ model—electronic properties

In order to evaluate induction effects, we calculated the partial, atomic charges of each atom in the dimer clusters and the resulting dipole moments. The changes in atomic charges and dipole moments upon complexation are listed in Table 2. The first, notable feature is that the positive partial charges of the lanthanide ions decrease in the dimer, indicating some (slight) electron transfer from the solvent.[2]

A significant distortion of the electronic distribution of the water molecule occurs due to the polarizing nature of the lanthanide ion, which pulls some negative charge from the oxygen atom. The extent of charge transfer from oxygen to the lanthanide ion is of the order of 0.15e for all ions studied. The electronic changes are accompanied by slight structural changes in the water molecule: the O–H bonds are elongated by 0.03 Å and the water bond angle shrinks by an average ∼1.6°. These results are in agreement with the trends previously reported by Hengrasmee et al. [26]. Induction effects result in a significant increase in the dipole moment of water, of the order of ∼1.2–1.4 D, which is substantially larger than the increase observed in clusters of smaller charge:size ratios [52,53]. These results clearly demonstrate the need to incorporate polarization into any model that accurately describes Ln^{3+}–water interactions.

2.4. Larger $Ln^{3+}(H_2O)_n$ clusters (n = 6, 8, and 9)

In addition to our benchmark with cluster dimers, we will compare the predictions of our model against quantum chemistry calculations for a select number of larger clusters. Based

[2] We note that the ESP method of Ref. [47] provides charge distributions that properly describe the electrostatic potential experienced by a spectator species such as another solvent molecule. ESP charges are thus adequate as the basis for parameterization of model potentials for ionic clusters, but may be questionable for discussing intermolecular charge transfer. We note however that other methods such as Mulliken charge analysis [64], Natural Bond Orbital theory [65] and the quantum theory of Atoms in Molecules [66] yield very similar results (S.R. Hughes, J.A. Capobianco, G.H. Peslherbe, On the Nature of Bonding Interactions in Small Metal Ion-Water Clusters, to be submitted).

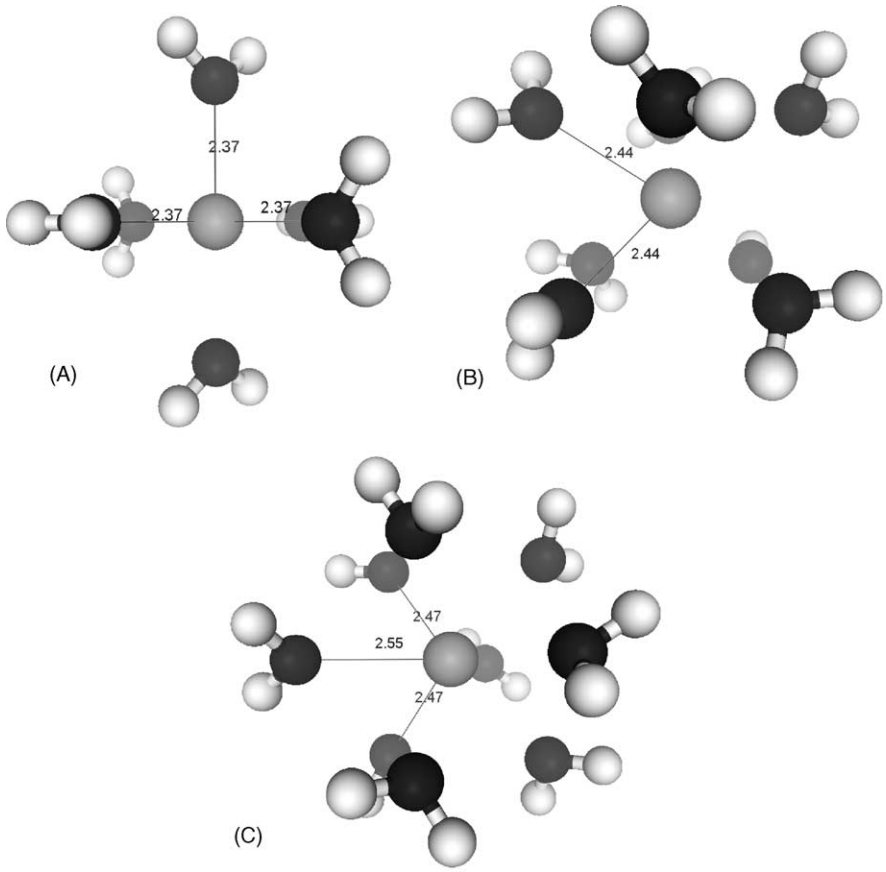

Fig. 1. Minimum energy $Er^{3+}(H_2O)_n$ cluster structures for (A) $n = 6$, (B) $n = 8$ and (C) $n = 9$ obtained from quantum chemistry calculations with the HF/SDD/6-31+G(2d,p) model chemistry. Distances are in Å.

on the fact that B3LYP seemed to systematically overestimate binding energies for the dimers by as much as 10% (cf. Table 1), we opted to perform HF calculations for the larger clusters. Even though HF lacks electron correlation, it yielded dimer structural and energetic properties comparable to those predicted by the high-level QCISD(T) and, as such, HF calculations may provide respectable estimates of the properties of large $Ln^{3+}(H_2O)_n$ clusters.

In previous work by Walker et al. [8], $Ho^{3+}(H_2O)_n$ were reportedly not found in mass spectrometry experiments employing the pick-up technique, but it was shown that metal–solvent clusters of various sizes containing acetonitrile or acetone could be generated. In particular, $Ho^{3+}(CH_3CN)_6$ and $Ho^{3+}(C_3H_6O)_6$ appeared to be preferentially formed. Accordingly, we have attempted to probe the characteristics of hexa-coordinated Ln^{3+} complexes via quantum chemistry calculations. An octahedral symmetry was assumed to be the initial structure, given that it is the preferential coordination of the lanthanide ions with 6 ligands [31]. An example of a minimized structure can be seen in Fig. 1 A and properties of these clusters are collected in Table 3. Similar trends are observed as for the dimer. For instance, the bond distances shorten from an average 2.50 Å in $Nd^{3+}(H_2O)_6$ to 2.33 Å in $Yb^{3+}(H_2O)_6$. Furthermore, the total cluster binding energies increase, from 371.0 to 431.2 kcal/mol for the same clusters.

We have also optimized the structures of $Ln^{3+}(H_2O)_8$ and $Ln^{3+}(H_2O)_9$, since these clusters correspond to the preferential coordination numbers of lanthanide ions in solution [28–32]. We assumed a square anti-prism (SQA) and a tri-capped trigonal prism (TCTP) for the 8- and 9-coordinated clusters, respectively (see Fig. 1B and C), as they appear to be the preferred coordination structures of water to the lanthanides in solution [28–32].[3] The features of these clusters are also collected in Table 3. The ion–water distances are seen to decrease across the lanthanide series, very much like what was observed earlier for the dimer model, reflecting the 'lanthanide contraction'. Our structural results compare well with those of Cosentino et al., who reported the features of several global minimum energy structures for $Nd^{3+}(H_2O)_8$, $Yb^{3+}(H_2O)_8$ and $Gd^{3+}(H_2O)_9$ clusters [23,24]. In addition our energetic results are in the range of those reported by Hengrasmee et al., though their calculations

[3] No systematic quantum chemistry investigation of the larger clusters was performed. The SQA and TCTP structures were only considered here as typical 8- and 9-coordinated cluster structures. They appear, however, to be the lowest-energy structures for such cluster sizes. For instance, the total cluster binding energy of the 7 + 1 coordinate $Eu^{3+}(H_2O)_8$ cluster is approximately 5 kcal/mol higher in energy than the SQA structure, and that of the 6 + 3 coordinate structure for $Eu^{3+}(H_2O)_9$ is 2 kcal/mol higher than the TCTP structure.

Table 3
Structural, energetic and electronic properties of $Ln^{3+}(H_2O)_n$ ($n = 6$, 8 or 9)

Ion	Property	6-coordinated		8-coordinated		9-coordinated	
		HF[a]	Model[b]	HF[a]	Model[b]	HF[a]	Model[b]
Nd^{3+}	r_{Ln-O}[c]	2.50	2.63	2.54	2.74	2.59/2.61	2.78/2.84
	U[d]	371.0	351.5	431.2	403.9	451.0	424.8
	μ_{H_2O}[e]	3.24	4.10	3.08	3.60	3.10/2.99	3.50/3.35
	q_{Nd}[e]	+2.8	+3.0	+2.9	+3.0	+3.0	+3.0
Eu^{3+}	r_{Ln-O}[c]	2.45	2.63	2.53	2.72	2.55/2.58	2.75/2.82
	U[d]	389.4	364.0	449.1	416.9	467.7	438.4
	μ_{H_2O}[e]	3.34	4.10	3.14	3.60	3.11/3.07	3.53/3.37
	q_{Eu}[e]	+2.8	+3.0	+3.1	+3.0	+3.2	+3.0
Er^{3+}	r_{Ln-O}[c]	2.36	2.63	2.44	2.67	2.47/2.54	2.69/2.78
	U[d]	419.4	392.2	477.4	451.9	493.7	471.3
	μ_{H_2O}[e]	3.27	4.10	3.09	3.70	3.16/3.11	3.56/3.37
	q_{Er}[e]	+2.8	+3.0	+2.9	+3.0	+2.8	+3.0
Yb^{3+}	r_{Ln-O}[c]	2.33	2.50	2.42	2.66	2.44/2.53	2.68/2.80
	U[d]	431.2	406.0	487.5	441.9	502.9	459.5
	μ_{H_2O}[e]	3.26	4.20	3.10	3.71	3.14/3.10	3.59/3.33
	q_{Yb}[e]	+2.8	+3.0	+2.9	+3.0	+3.0	+3.0

[a] Quantum chemistry calculations are performed with the 6-31+G(2d,p)/SDD basis set as discussed in the text.
[b] Predictions of model potentials.
[c] Lanthanide to oxygen distance (Å). For 9-coordinated species, the values listed correspond to the axial and equatorial ligand properties, respectively.
[d] Binding energy (kcal/mol) corrected for zero-point energy and basis-set superposition error.
[e] Dipole moment (D) of water and atomic charges of Ln^{3+} (e) based on calculated ESP charges [47]. For 9-coordinate species, the values listed correspond to the axial and equatorial ligand properties, respectively.

assumed a cubic structure for $Ln^{3+}(H_2O)_8$ as opposed to the SQA structure [26]. HF calculations for the $Ln^{3+}(H_2O)$ dimer seemed to underestimate the cluster binding energies by a consistent ~4 kcal/mol (approximately 4%), compared to the QCISD(T) predictions. Thus, the HF energies listed in Table 3 may also be underestimated by a similar 4%.

3. Model potential and simulations/procedure

3.1. Functional form of the model potentials

The model chosen to represent ion–water and water–water interactions is a sum of Coulombic, induction and repulsion-dispersion terms [1–3]:

$$U = U_{\text{Coulomb}} + U_{\text{Induction}} + U_{\text{Repulsion-dispersion}}. \quad (1)$$

The Coulombic energy simply reflects the interactions between permanent charges:

$$U_{\text{Coulomb}} = \sum_{i,j} \frac{q_i q_j}{r_{ij}}, \quad (2)$$

where i and j represent different sites in the system separated by a distance r_{ij} and the q's are the static point charges of the metal ion and the water atoms. The induction energy is expressed as

$$U_{\text{Induction}} = -\frac{1}{2}\sum_i \vec{E}_i^{\,0}\vec{\mu}_i, \quad (3)$$

where E_{ij} is the electric field at site i arising from the permanent charges:

$$\vec{E}_i^{\,0} = \sum_j \frac{q_j \cdot \vec{r}_j}{|\vec{r}_i - \vec{r}_j|^3}, \quad (4)$$

and the induced dipoles, μ_{ij}, are evaluated as a linear response to the total electric field:

$$\vec{\mu}_i = \alpha_i \cdot \vec{E}_i = \alpha_i \left[\vec{E}_i^{\,0} + \sum_{i\neq j} T_{ij} \cdot \vec{\mu}_j\right], \quad (5)$$

where α_i is the polarizability of site i and T_{ij} is the dipole tensor [54]. The polarizable sites in the induced dipole problem of Eqs. (3) to (5) account for the mutual polarization of the solvent molecules and the lanthanide ion. In cluster simulations, the low dimensionality of the problem yields a straightforward solution of the set of linear equations in Eq. (5) in matrix form [55], which is obtained by LU decomposition and back substitution [56] in this work. The repulsion-dispersion interactions are represented by a generalized 12-8-6 Lennard-Jones potential:

$$U_{\text{Repulsion-dispersion}} = \sum_{i,j}[A_{ij}r_{ij}^{-12} + B_{ij}r_{ij}^{-8} - C_{ij}r_{ij}^{-6}], \quad (6)$$

where A_{ij}, B_{ij} and C_{ij} are adjustable parameters.

3.2. Parameterization of the model potentials

The parameters for the polarizable model include the point charges (q_i), the polarizabilities (α_i) and the repulsion-

Table 4
Potential parameters

	A_{ij}[a]	B_{ij}[a]	C_{ij}[a]
Nd^{3+}–O	0	92665	7099
Eu^{3+}–O	0	93199	7871
Er^{3+}–O	0	92488	9327
Yb^{3+}–O	0	77694	6794
O–O[b]	1,152,921	0	1074
H–H[b]	10^{5}[c]	5.5[c]	

	α[d]	q[e]
Nd^{3+}	2.8	3.00
Eu^{3+}	2.8	3.00
Er^{3+}	2.8	3.00
Yb^{3+}	2.8	3.00
O[b]	1.45	−0.569
H[b]	–	0.569

	r_{O-M}[f]	θ_{H_2O-M}[g]
Water	0.342	43.4

[a] Repulsion-dispersion parameters: A_{ij} (kcal mol Å^{-12}), B_{ij} (kcal mol Å^{-8}), C_{ij} (kcal mol Å^{-6}).
[b] From references [1,2].
[c] Repulsion parameters between hydrogen atoms: the functional form of this interaction is a Born-Mayer term, $A_{ij}e^{-B_{ij}r}$, with parameters A_{ij} (kcal/mol) and B_{ij} (Å^{-1}) [1].
[d] Polarizability (Å^3).
[e] Permanent point charges (e).
[f] Distance between oxygen and its charge sites (Å) [1].
[g] Angle defining each oxygen charge site with respect to the molecular plane of water (°).

dispersion parameters (A_{ij}, B_{ij}, and C_{ij}). The lanthanide ions are assigned a +3 charge and a polarizability of 2.8 Å^3. The latter is larger than the experimental polarizability of La^{3+} (1.6 Å^3) [57] and should be more representative of that for the late ions in the lanthanide series. The point charges and polarizability of water are those of our OPCS model [1,2]. The parameters are listed in Table 4. Briefly, the OPCS model is a rigid, 5-site model, with 4 permanent charge sites, one induced dipole site on the oxygen atom and repulsion sites on the hydrogen atoms. Of the 4 permanent charges, 2 positive charges are positioned on the hydrogen atoms, while 2 negative charges are located in the vicinity of the oxygen atom towards the hydrogen atoms, out of plane from the water symmetry axis. It should be noted that this model employs a water molecule with a rigid gas-phase geometry (r_{OH} = 0.9572 Å, $\angle_{HOH}$ = 104.52° [58]) and reproduces the gas-phase water dipole moment [59]. The repulsion-dispersion parameters for the solvent–solvent interactions were fit to reproduce the water dimer geometry and binding energy [1]. The ion–solvent interactions were fit to reproduce the equilibrium ion–water distance, the binding energy and the dipole moment of water molecules as predicted by quantum chemistry calculations for the ion–water dimer. This fitting was performed using a non-linear least-squares algorithm based on the Marquardt-Levenberg method [56].

Table 1 lists the structural, energetic and electronic properties of the ion–water dimer minimum energy structure predicted by the model potentials. We note that the binding energies of the dimers are reproduced very well by our model potentials, with little or no deviation with respect to the QCISD(T) values. The ion–water bond distances differ from the MP2 value by at most 0.08 Å, which constitutes an overall error of only 3% with respect to the quantum chemistry reference. The water dipole moments predicted by our model potentials follow the trend predicted by our quantum chemistry calculations, i.e., they are significantly larger than that of gas-phase water in the presence of lanthanide ions, and lighter lanthanide ions have a smaller effect on the induced dipole than heavier ions. However, the water dipole moments in $Ln^{3+}(H_2O)$ clusters are grossly overestimated by our model potential when compared to the quantum chemistry results. Improving the water dipole moments predicted by the model potentials could only be done at the expense of the cluster structure and binding energy. This overestimate of solvent polarization in the dimer may be attributed to the neglect of charge transfer in the functional form of the potential, but as will be discussed shortly, it will be less of an issue for larger clusters.

The predictions of our model potentials for a select number of larger $Ln^{3+}(H_2O)_n$ clusters (n = 6, 8, and 9) are summarized in Table 3, where they are compared to the results of quantum chemistry calculations. The ion–water distances predicted by the model potentials across the lanthanide series parallel the quantum chemistry results, and again reflect the 'lanthanide contraction' phenomenon. It can also be seen that the water dipole moments decrease significantly compared to their value in the cluster dimer, and in general decrease with cluster size increase. We also note that the overestimation of the water dipole moments by the model potentials, compared to the quantum chemistry results, is greatly reduced in larger clusters, for which the predictions of the model potential lie within ∼20% of the quantum chemistry results. This is due to the ion making multiple associations with solvent molecules and an increased number of solvent–solvent repulsions, which result in structures with the ion located at a larger distance from the water molecules. For instance, the average ion–oxygen distance is ∼0.2 Å longer for cluster size 6 when compared to those for cluster size 1, and the larger distances between the ion and the solvent molecules naturally lead to a decrease of mutual polarization. In addition, it can be seen from Table 3 that the atomic charge of the lanthanide ion increases with cluster size, regaining the full +3 charge by cluster size 9. This clearly indicates that charge transfer is not an issue for larger clusters and that, even though polarization effects may be overestimated for smaller clusters, they will be quantitatively described by our model potential for medium-size to large clusters. At n = 6, 8 and 9, the water molecules are located at much larger distances from the ion with respect to those seen in the dimer (∼0.2 Å further). For this reason, the charge transfer mechanism becomes less probable and thus, is minimized in our calculations of larger clusters.

Finally, inspection of Table 3 reveals that the model potentials seem to properly account for many-body interactions,

yielding cluster binding energies underestimated by only 6% compared to the quantum chemistry values for intermediate cluster sizes 6, 8 and 9. Together with the fact the HF quantum chemistry results underestimated the binding energies predicted by high-level QCISD(T) calculations by 4%, this suggests an error bar of ∼10% for energetic properties predicted by our model potentials for medium-size clusters.

3.3. Monte Carlo simulations

Monte Carlo simulations were used to investigate the thermodynamic and structural properties of $Ln^{3+}(H_2O)_n$ clusters at 300 K. The detailed procedure has been reported previously [3] and only the key features are summarized here. A random-walk approach is used to generate new configurations, which involves the random translation of a water molecule in Cartesian space and its rotation around the Euler angles. The maximum allowed translations were set to 0.15 Å and the range of angular movements was set to 15°. The resulting configurations were accepted or rejected according to the Metropolis algorithm [60]. Because we are simulating clusters and not the bulk liquid, no periodic boundary conditions were imposed. As a consequence, evaporation of the solvent molecules from the cluster is possible and it was closely monitored. Any water molecule that is found beyond 20 Å from the ion for cluster sizes $n < 64$ and 35 Å for clusters sizes $64 \leq n < 128$ are considered evaporated from the cluster. Markov chains containing configurations with evaporated solvent molecules were discarded from the overall sampling so as to define a representative, equilibrium ensemble for a given cluster size. A periodic heating and cooling of the system was used to avoid trapping in local minima. In general, each run entailed at least 2×10^6 configurations for equilibration, followed by an equal amount of steps for data collection. The acceptance ratios obtained ranged between 35 and 45%.

Cluster enthalpies were calculated from the average energy $\langle U \rangle$ of the canonical ensembles of configurations as

$$\Delta H_n = \Delta U + \Delta(PV) = \langle U \rangle + nRT, \quad (8)$$

and the stepwise binding enthalpies, which represent the enthalpy gain associated with the addition of one solvent molecule to the cluster, were calculated as

$$\Delta H_{n,n-1} = \Delta H_n - \Delta H_{n-1}. \quad (9)$$

The structural properties of the clusters were analyzed in terms of a distance-dependent coordination number $N_{coord}(r)$, and its derivative, $P(r)$, which is the normalized radial probability distribution function:

$$P(r) = \frac{dN_{coord}(r)}{dr} = \frac{n4\pi r^2 g(r)}{\int_0^\infty 4\pi r^2 g(r)\,dr} \quad (10)$$

It should be noted that $P(r)$ differs from the radial distribution function $g(r)$ used in liquid structure theory by a factor of $4\pi r^2$ and it is normalized to the number of solvent molecules in the cluster.

4. Results and discussion

4.1. Structural data

Fig. 2 shows some representative structures of $Eu^{3+}(H_2O)_n$ clusters obtained from room-temperature Monte Carlo simulations. The ion is clearly coordinated to the water oxygen atoms and the clusters exhibit an interior solvation shell structure. The latter finding is further ascertained from the probability distribution functions shown in Fig. 3, where clear peaks are indicative of a well-defined ion solvation shell structure. The interior solvation structure is due to the fact that the loss in free energy associated with the disruption of the solvent network is compensated by the formation of much stronger ion–solvent bonds. This is not surprising given the very large lanthanide ion–water binding energies discussed earlier, of the order of 100 kcal/mol, compared to a water–water interaction energy of ∼5 kcal/mol [1]. Evidence of a second, loose, coordination shell can be seen for large clusters such as $Ln^{3+}(H_2O)_{64}$ from the second peak at ∼5 Å. This is a reflection of the long-range influence of the ion on the solvent and indicates that the ion–solvent interactions ultimately govern the cluster structure.

The probability distribution functions shown for $Ln^{3+}(H_2O)_{64}$ are representative of those observed for all clusters $n \geq 24$ for each ion studied. In the case of Eu^{3+}, where the average first-shell coordination number lies between 8 and 9, simulation results point to a purely 8- or 9-coordinated first hydration shell structure. Furthermore, the fact that the probability distribution function, $P(r)$, goes to zero in between the two peaks representing the first and second coordination shells indicates that solvent molecules are not found in between the coordination shells, in agreement with the low residence times for water previously reported by Kowall et al. [38,39].

The average first-shell coordination numbers of the lanthanide ions are listed in Table 5 for a number of cluster sizes. When approaching cluster size 64, the coordination numbers derived from our simulations agree well with those obtained from X-ray and neutron diffraction experiments of $LnCl_3$ solutions [28–32], and changes in coordination numbers along the series are consistent with solution experimental data. The relatively slow convergence of the coordination numbers to the bulk values contrasts with what was observed

Table 5
Average first-shell coordination numbers of $Ln^{3+}(H_2O)_n$

	n									Exp[a]
	6	7	8	9	12	24	36	64	128	
Nd^{3+}	6.0	6.6	6.5	6.5	6.4	8.0	8.0	8.2	8.6	8.9
Eu^{3+}	6.0	7.0	7.0	6.9	7.0	8.0	8.0	8.2	8.4	8.3
Er^{3+}	6.0	6.9	7.1	7.0	6.7	7.8	8.0	8.0	8.0	8.2
Yb^{3+}	6.0	6.3	7.3	6.6	7.1	7.9	7.9	7.9	8.4	7.9

[a] Bulk solution data [28–32].

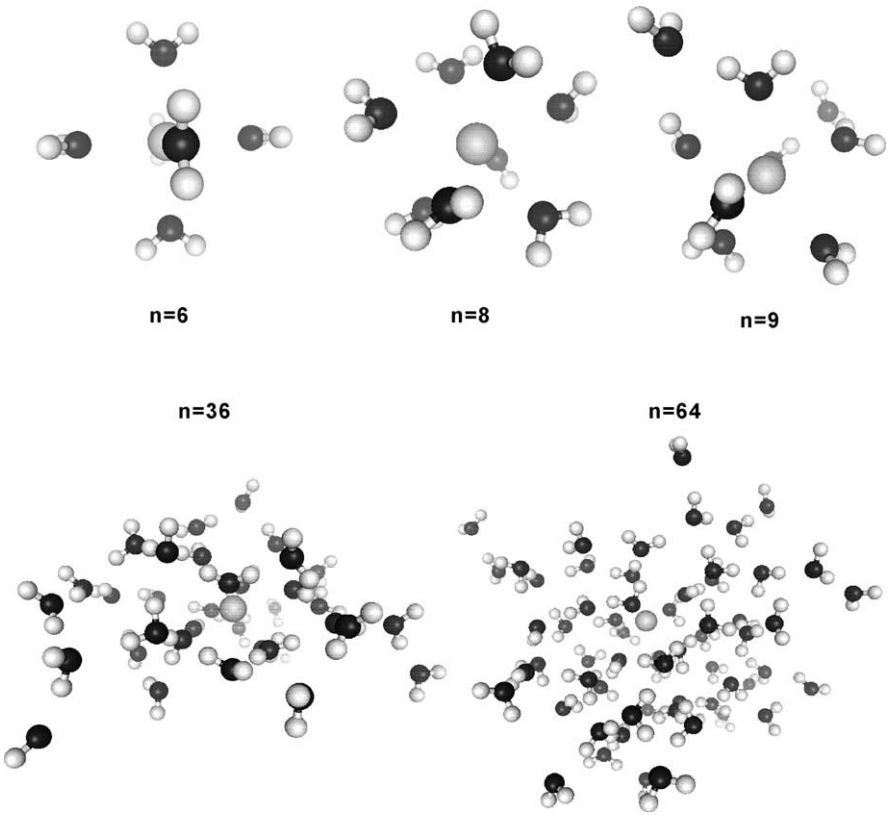

Fig. 2. Representative structures obtained for $Eu^{3+}(H_2O)_n$ clusters from Monte Carlo simulations with model potentials.

in our previous work on cesium and sodium–water clusters [1–3], for which the coordination numbers are comparable to those observed in the bulk at very small cluster sizes ($n < 12$). This difference is due to the low charge:size ratio of the monovalent ions, which results in weaker ion–water interaction energies. For instance, the binding energy of sodium to water is ~24 kcal/mol, whereas that of ytterbium to water is ~106 kcal/mol. As a result, first-coordination shell water molecules can be found at a larger distance from the ion and from each other, and solvent–solvent repulsions in the first coordination shell are minimized in monovalent ion–water clusters.

The distances between the ions and the oxygen atoms of the water molecules in the first coordination shell are listed in Table 6 for a number of cluster sizes. Experimental, bulk values from diffraction studies of $LnCl_3$ salt solutions are also provided in Table 6 for comparison [28–32]. The cluster ion–water distances, even for very large clusters, are larger than those for bulk solutions by 0.25 Å. These deviations could be attributed to the absence of counter-ions in our clusters, which may drive the solvent to coordinate more tightly to the cations due to repulsions. Compared to the previous model of Floris and Tani [25], our model reproduces the decrease of the coordination number across the series, but apparently at the expense of the ion–water distances. Both the models of Floris and Tani [25] and Kowall et al. [38] failed to describe the solvation of Yb^{3+} in solution appropriately. The former failed to reproduce the experimental coordination number and the latter, the ion–water distance in the bulk. Our model not only manages to reproduce the appropriate coordination number of Yb^{3+}, but the trend in the Yb^{3+}–O distance predicted for large clusters by our model also is consistent with the experimental bulk values [28–32]. Our model is thus capable of consistently describing the qualitative differences in lanthanide coordination across the series.

Solvation in smaller clusters differs somewhat from that for larger clusters. Inspection of Table 5 indicates that the model predicts either 6 + 2 or 7 + 1, and either 6 + 3 or 7 + 2 coordination for cluster sizes 8 and 9, respectively. The +1,

Table 6
Average ion–water distance (Å) in the first coordination shell of $Ln^{3+}(H_2O)_n$[a]

	N				Exp[b]
	24	36	64	128	
Nd^{3+}	2.74	2.73	2.75	2.77	2.51
Eu^{3+}	2.72	2.71	2.71	2.74	2.45
Er^{3+}	2.65	2.66	2.66	2.65	2.37
Yb^{3+}	2.64	2.64	2.63	2.67	2.32

[a] Average lanthanide to oxygen distance from Monte Carlo simulations. The cut-off radius for the first coordination shell was determined from the probability distribution functions.
[b] Bulk solution data [28–32].

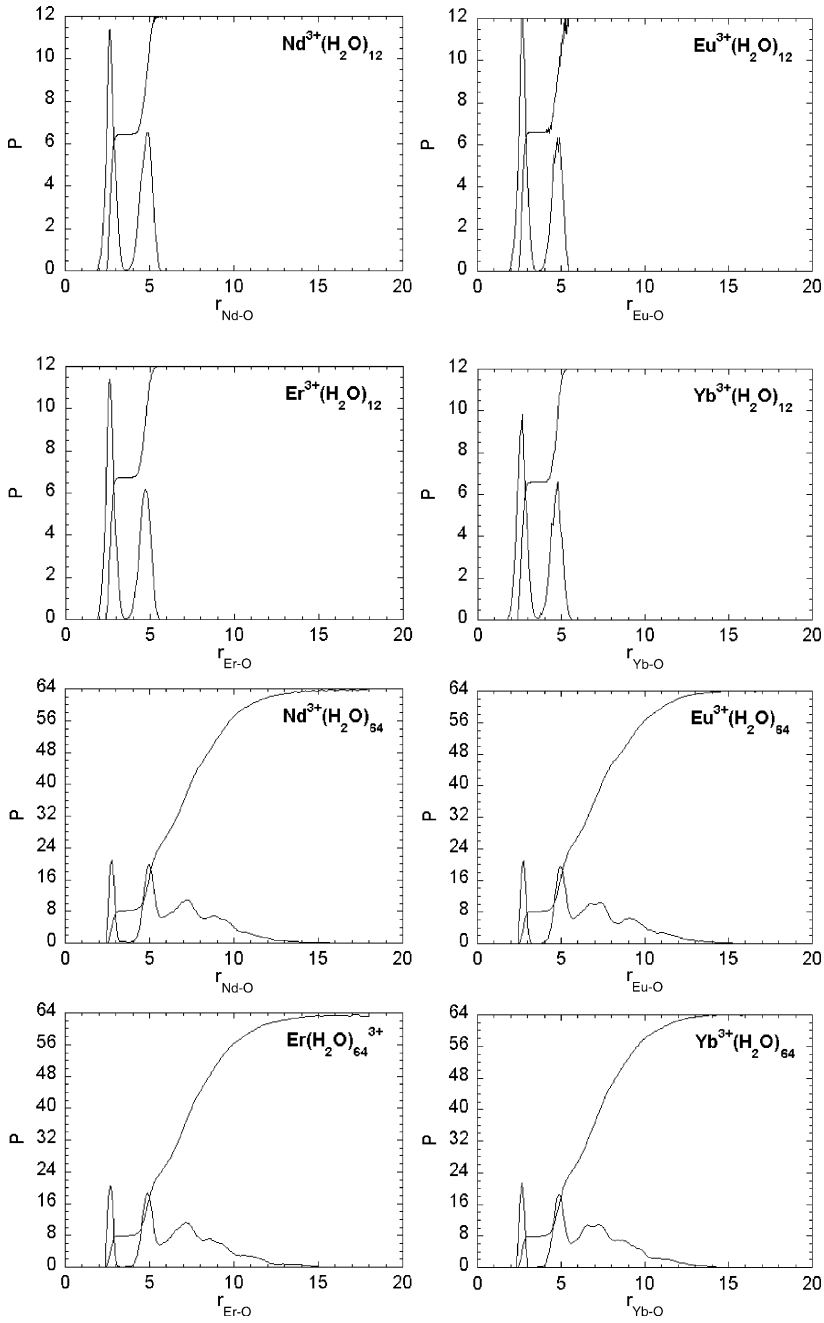

Fig. 3. Radial probability distribution functions and cumulative radial probability distribution functions vs. Ln^{3+}–O distance for $Ln^{3+}(H_2O)_{12}$ and $Ln^{3+}(H_2O)_{64}$ ($Ln^{3+} = Nd^{3+}$, Eu^{3+}, Er^{3+} and Yb^{3+}). First-shell coordination numbers derived from the cumulative functions are listed in Table 5 and average ion–oxygen distances in Table 6.

+2 and +3 refer to solvent molecules that reside outside the first coordination shell, indicating the beginning of a second hydration shell formation. This trend is observed for all clusters in the range of $n = 8$–12. This is not a surprising result since no solvent network is present to confine the additional solvent molecules in the first solvation shell. At larger cluster sizes, additional solvent molecules may drive the ion coordination numbers towards bulk values. Similar behavior has been reported by Derepas et al. [5] for small $La^{3+}(H_2O)_n$ clusters.

4.2. Thermodynamic data

Cluster enthalpies for $Ln^{3+}(H_2O)_n$ clusters are shown as a function of clusters size in Fig. 4. We note that since our model potentials are likely to underestimate the cluster binding energies by ∼10% for medium-sized clusters (cf. Section 3.2), the total cluster enthalpies are likely to be underestimated by a similar 10%. Stepwise binding enthalpies for cluster sizes $n = 6$–15 are shown in Fig. 4a. A remarkable feature of the stepwise binding enthalpies is the more pronounced decrease

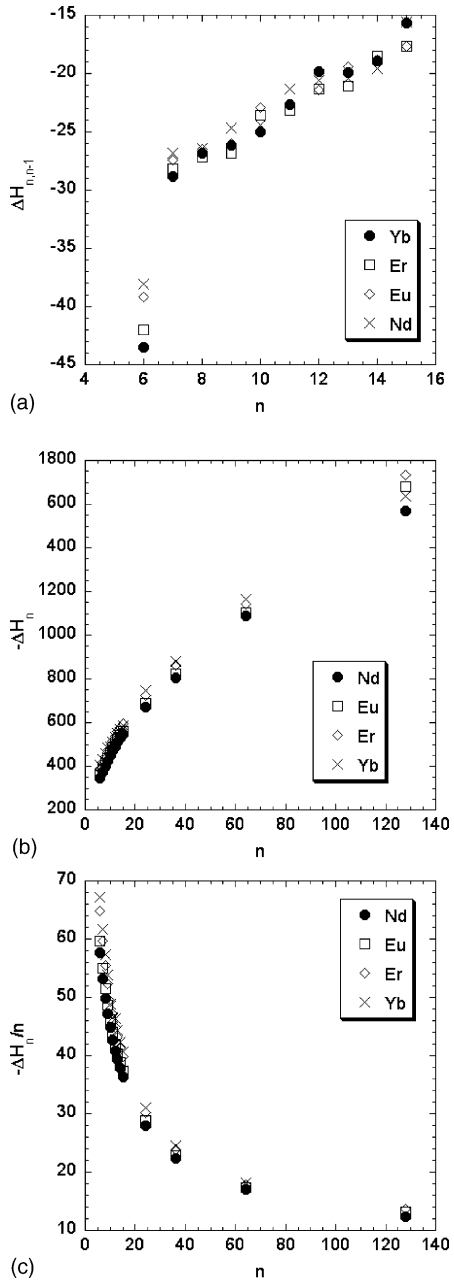

Fig. 4. (a) Stepwise binding enthalpy vs. cluster size for $Ln^{3+}(H_2O)_n$ clusters (n = 6–15); (b) reduced cluster enthalpy vs. cluster size for $Ln^{3+}(H_2O)_n$ clusters (n = 6–128). The experimental heat of vaporization of bulk water, shown as a dashed line, has a value of 9.7 kcal/mol; (c) total cluster enthalpy vs. cluster size for $Ln^{3+}(H_2O)_n$ clusters (n = 6–128). All enthalpies are in kcal/mol.

occurring between $\Delta H_{6,5}$ and $\Delta H_{7,6}$, which coincides with the completion of the first hydration shell in small clusters as shown in Fig. 3 (top panels) and as discussed earlier. Since the solvation of Ln^{3+} ions in both water and acetonitrile in the bulk follow similar trends [61], a similar behavior may be expected for small clusters, and these findings may be consistent with the experimental observations of only $Ho^{3+}(C_3H_6O)_6$ and $Ho^{3+}(CH_3CN)_6$ clusters [8].

Total cluster enthalpies and reduced cluster enthalpies are shown in Fig. 4b and c, respectively, as a function of cluster size. The thermodynamic properties follow the energetic trends observed earlier, with the lighter lanthanide ions having smaller cluster enthalpies than the heavier ions. For example, the $Nd^{3+}(H_2O)_{128}$ cluster has a total enthalpy of ∼1492 kcal/mol, whereas the $Yb^{3+}(H_2O)_{128}$ cluster has a total enthalpy of ∼1556 kcal/mol. At a cluster size $n \geq 36$, the total cluster enthalpies start to increase almost linearly. This may reflect the decreasing influence of the ion interaction with the outermost solvent molecules and indicate that the change in stabilization enthalpy of the cluster arises primarily from additional H_2O–H_2O interactions. This is reflected in the plateau observed in the reduced cluster enthalpy shown in Fig. 4c. The latter converges to the heat of vaporization of water, whose experimental value is around 9.7 kcal/mol [62],[4] as the reduced cluster enthalpy naturally approaches the average amount of energy necessary to vaporize one solvent molecule from the cluster in the large cluster regime [3]. The reduced cluster enthalpies for $Ln^{3+}(H_2O)_n$ are ∼17.0 kcal/mol for n = 64 and ∼13.0 kcal/mol for n = 128. Interestingly, the convergence of the reduced cluster enthalpy towards the heat of vaporization of water occurs at a far faster rate in clusters containing smaller monovalent metal ions than in those containing trivalent lanthanides. For instance, the $Na^{+}(H_2O)_{36}$ reduced cluster enthalpy lies only within ∼2 kcal/mol of the heat of vaporization of water [3]. This is once again a reflection of the long-range influence of the trivalent lanthanide ion interaction with the surrounding solvent molecules beyond the first coordination shell.

5. Conclusions

In this work, we have investigated the structural and thermodynamic properties of $Ln^{3+}(H_2O)_n$ clusters by means of room-temperature Monte Carlo simulations. These calculations made use of a rigorous model potential containing an explicit polarization term that was fitted to quantum chemistry predictions of the energetic, structural and electronic properties of small Ln^{3+}–water clusters.

An interior solvation shell structure is observed for all $Ln^{3+}(H_2O)_n$ clusters, and peaks in the probability distribution functions indicate a well-defined solvation shell structure. For all clusters, the following trends are observed in going across the lanthanide series: ion–water binding energies increase, while ion–water distances decrease. Smaller clusters (n = 8–12) tend to adopt 6- or 7-coordinated structures due to the absence of a solvent network, which influences the coordination number via induction effects. At large cluster sizes, the lighter lanthanide ions (e.g., Nd^{3+}) show a preference for forming 9-coordinated structures with their ligands, whereas the heavier lanthanides (e.g., Yb^{3+}) yield

[4] Liquid simulations are being performed in order to assess how well our model potential can reproduce the heat of vaporization of water.

8-coordinated structures, in agreement with what is observed experimentally for bulk solution [28–32].

Since there has been little experimental work on multiply charged ion aqueous clusters, we have calculated thermodynamic quantities related to the binding of water molecules to Ln^{3+} ions to guide possible, future experiments. The predicted stepwise binding enthalpies are quite large, even for small cluster sizes. A more pronounced decrease of the stepwise binding enthalpies occurs between $n = 6$ and 7, reflecting the completion of the first coordination shell in small clusters and indicating the higher stability of hexa- and hepta-coordinated clusters, a feature consistent with experimental observations with other solvents [8]. The total cluster enthalpies show that the lighter lanthanides bind less tightly to the solvent than do the heavier ions. At larger cluster sizes, the increase in the cluster enthalpies is attributed to interactions of the additional (outermost) water molecules with other solvent molecules that solvate the ion. As a result, the reduced cluster enthalpies converge to the heat of vaporization of liquid water but the rate of convergence for $Ln^{3+}(H_2O)_n$ is much slower than what was observed for monovalent ion aqueous clusters [1–4], a feature consistent with the strong, long-range interaction of Ln^{3+} ions with solvent molecules.

Previous simulations of monovalent metal ion aqueous clusters, following the same procedure and employing similar model potentials as in this work, yielded stepwise binding energies in excellent agreement with available experimental data [1–4]. This gives confidence in the predicted thermodynamic quantities reported in this work, which in turn could serve as benchmarks for future mass spectrometry experiments. This work is being extended to explore the solvation of Ln^{3+} metal ions with other solvents, such as acetonitrile, for which a stable hexa-coordinated cluster has been reported [8]. The model potentials are also being refined to account for charge transfer between ions and solvent molecules via the incorporation of fluctuating charges [63], and by improving the treatment of polarization. Finally, a systematic quantum chemistry investigation of larger clusters and first-principles lanthanide–solvent simulations are underway to gain more insight into why the retention of the 3+ state of lanthanide ions has been observed experimentally in acetonitrile clusters, but not in water clusters.

Acknowledgements

This research was supported by the Natural Sciences and Engineering Research Council (NSERC) of Canada and the Fonds Québeçois de la recherche sur la nature et les technologies (FQRNT). Calculations were done at the Centre for Research in Molecular Modeling (CERMM), which was established with the financial support of the Concordia University Faculty of Arts and Science, the Ministère de l'Éducation du Québec (MEQ) and the Canada Foundation for Innovation (CFI). GHP holds a Concordia University Research Chair. The authors would like to thank anonymous reviewers for very helpful and insightful comments.

References

[1] G.H. Peslherbe, B.M. Ladanyi, J.T. Hynes, J. Phys. Chem. A 104 (2000) 4533.
[2] G.H. Peslherbe, B.M. Ladanyi, J.T. Hynes, Chem. Phys. 258 (2000) 201.
[3] T.-N.V. Nguyen, G.H. Peslherbe, J. Phys. Chem. A 107 (2002) 1540.
[4] D.M. Koch, G.H. Peslherbe, Chem. Phys. Lett. 359 (2002) 381.
[5] A.-L. Derepas, J.-M. Soudan, V. Brenner, J.-P. Dognon, P.J. Millie, J. Comput. Chem. 23 (2002) 1013.
[6] A.J. Stace, Phys. Chem. Chem. Phys. 3 (2001) 1935.
[7] D. Vukomanovic, J.A. Stone, Int. J. Mass Spectrom. 202 (2000) 251.
[8] N.R. Walker, R.R. Wright, A.J. Stace, C.A. Woodward, Int. J. Mass Spectrom. 188 (1999) 113.
[9] A.T. Blades, P. Jayaweera, M.G. Ikonomou, P. Kebarle, Int. J. Mass Spectrom. Ion Process. 101 (1990) 325.
[10] Z.L. Cheng, K.W.M. Siu, R. Guevremont, S.S. Berman, Org. Mass Spectrom. 27 (1992) 1370.
[11] A.A. Shvartsburg, J. Am. Chem. Soc. 124 (2002) 7910.
[12] A.A. Shvartsburg, Chem. Phys. Lett. 360 (2002) 479.
[13] A.A. Shvartsburg, J. Am. Chem. Soc. 12 (2002) 12343.
[14] I.I. Stewart, G. Horlick, Anal. Chem. 66 (1994) 3983.
[15] T. Kojima, I. Kudaka, T. Sato, T. Asakawa, R. Akiyama, Y. Kawashima, K. Hiraoka, Rapid Commun. Mass Spectrom. 13 (1999) 2090.
[16] A.T. Blades, P. Jayaweera, M.G. Ikonomou, P.J. Kebarle, Chem. Phys. 92 (1990) 5900.
[17] R.R. Wright, N.R. Walker, S. Firth, A.J. Stace, J. Phys. Chem. A 105 (2001) 54.
[18] S.E. Rodriguez-Cruz, R.A. Jockusch, E.R. Williams, J. Am. Chem. Soc. 121 (1999) 1986.
[19] Y. Okuno, J. Phys. Chem. A 103 (1999) 190.
[20] T. Asada, K. Nishimoto, Chem. Phys. Lett. 232 (1995) 518.
[21] J.-C.G. Bünzli, N. André, M. Elhabiri, G. Muller, C. Piguet, J. Alloys Compd. 303–304 (2000) 66.
[22] W. Meier, P. Bopp, M.M. Probst, E. Spohr, J.-I. Lin, J. Phys. Chem. 94 (1990) 4672.
[23] U. Cosentino, G. Moro, D. Pitea, L. Calabi, A. Maiocchi, J. Mol. Struct. Theochem. 392 (1997) 75.
[24] U. Cosentino, A. Villa, D. Pitea, G. Moro, V. Barone, J. Phys. Chem. B 104 (2000) 8001.
[25] F.M. Floris, A. Tani, J. Chem. Phys. 115 (2001) 4750.
[26] S. Hengrasmee, M.M. Probst, Z. Naturforsch. 46a (1991) 117.
[27] H.J. Seifert, S. Funke, Thermochim. Acta 320 (1998) 1.
[28] A. Habenschuss, F.H. Spedding, J. Chem. Phys. 70 (1979) 3758.
[29] A. Habenschuss, F.H. Spedding, J. Chem. Phys. 70 (1979) 2797.
[30] A. Habenschuss, F.H. Spedding, J. Chem. Phys. 73 (1980) 442.
[31] E.N. Rizkalla, G.R. Choppin, in: K.A. Gschneider Jr., L. Eyring (Eds.), Handbook on the Physics and Chemistry of Rare-Earths, vol. 15, Elsevier Science Publishers B.V., New York, 1991, p. 393.
[32] E.N. Rizkalla, G.R. Choppin, in: K.A. Gschneider Jr., L. Eyring (Eds.), Handbook on the Physics and Chemistry of Rare-Earths, vol. 18, Elsevier Science Publishers B.V., New York, 1994, p. 529.
[33] Y. Marcus, in: R. Warncke (Eds.), Gmelin Handbuch der Anorganischen Chemie, vol. D1, New York, 1981, p. 1.
[34] V. Haase, H.K. Kugler, M. Lehl-Thalinger, U. Trobisch-RauBendorf, in: R. Warncke (Eds.), Gmelin Handbuch der Anorganischen Chemie, New York, 1979, p. 1.
[35] L. Helm, F. Foglia, T. Kowall, A.E. Merbach, J. Phys.: Condens. Matter 6 (1994) A137.
[36] S. Galera, J.M. Lluch, A. Oliva, J. Bertrán, F. Foglia, L. Helm, A.E. Merbach, N. J. Chem. 17 (1993) 773.

[37] C. Cossy, A.E. Merbach, Pure Appl. Chem. 60 (1988) 1785.
[38] T. Kowall, F. Foglia, L. Helm, A.E. Merbach, J. Am. Chem. Soc. 117 (1995) 3790.
[39] T. Kowall, F. Foglia, L. Helm, A.E. Merbach, J. Phys. Chem. 99 (1995) 13078.
[40] M.J. Frisch, G.W. Trucks, H.B. Schlegel, G.E. Scuseria, M.A. Robb, J.R. Cheeseman, V.G. Zakrzewski, J.A. Montgomery Jr., R.E. Stratmann, J.C. Burant, S. Dapprich, J.M. Millam, A.D. Daniels, K.N. Kudin, M.C. Strain, O. Farkas, J. Tomasi, V. Barone, M. Cossi, R. Cammi, B. Mennucci, C. Pomelli, C. Adamo, S. Clifford, J. Ochterski, G.A. Petersson, P.Y. Ayala, Q. Cui, K. Morokuma, D.K. Malick, A.D. Rabuck, K. Raghavachari, J.B. Foresman, J. Cioslowski, J.V. Ortiz, B.B. Stefanov, G. Liu, A. Liashenko, P. Piskorz, I. Komaromi, R. Gomperts, R.L. Martin, D.J. Fox, T. Keith, M.A. Al-Laham, C.Y. Peng, A. Nanayakkara, C. Gonzalez, M. Challacombe, P.M. W. Gill, B. Johnson, W. Chen, M.W. Wong, J.L. Andres, C. Gonzalez, M. Head-Gordon, E.S. Replogle, J.A. Pople, Gaussian 98, A.9 ed., Gaussian, Inc., Pittsburgh, 1998.
[41] W.J. Hehre, L. Radom, P.V.R. Schleyer, J.A. Pople, Ab Initio Molecular Orbital Theory, John Wiley & Sons, New York, 1985.
[42] I.N. Levine, Quantum Chemistry, Prentice Hall Inc., Englewood Cliffs, NJ, 1991.
[43] A.D. Becke, J. Chem. Phys. 98 (1993) 5648.
[44] J.A. Pople, M. Head-Gordon, K. Raghavachari, J. Chem. Phys. 87 (1987) 5968.
[45] S.F. Boys, F. Bernardi, Mol. Phys. 19 (1970) 553.
[46] M.J. Frisch, J.A. Pople, J.S. Binkley, J. Chem. Phys. 80 (1984) 3265.
[47] B.H. Besler, K.M. Merz Jr., P.A. Kollman, J. Comput. Chem. 11 (1990) 431.
[48] M. Dolg, H. Stoll, H. Preuss, J. Chem. Phys. 90 (1989) 1730.
[49] M. Dolg, H. Stoll, A. Savin, H. Preuss, Theor. Chim. Acta 75 (1989) 173.
[50] Q.K. Timerghazin, T.-N. Nguyen, G.H. Peslherbe, J. Chem. Phys. 116 (2002) 6867.
[51] Q.K. Timerghazin, G.H. Peslherbe, Halide Anions in a Methyl Pocket: Competition Between Hydrogen Bonding and Ion–Dipole Interactions in Acetonitrile–Halide Complexes, (submitted for publication).
[52] E.D. Glendening, J. Am. Chem. Soc. 118 (1996) 2473.
[53] E.D. Glendening, D. Feller, J. Phys. Chem. 100 (1996) 4790.
[54] L.X. Dang, T.M. Chang, J. Chem. Phys. 106 (1997) 8149.
[55] L. Perera, F.G. Amar, J. Chem. Phys. 90 (1989) 7364.
[56] W.H. Press, S.A. Teulkolsky, W.T. Vetterling, B.P. Flannery, Numerical Recipes, The Art of Scientific Computing, Cambridge University Press, Cambridge, 1992.
[57] C.K. Jørgensen, Struct. Bond. 1 (1966) 234.
[58] W.S. Benedict, N. Gailar, E.K. Plyler, J. Chem. Phys. 24 (1956) 1139.
[59] D.R. Lide, CRC Handbook of Chemistry and Physics, 77th ed., CRC, Boca Raton, Florida, 1996.
[60] N. Metropolis, A.W. Rosenbluth, M.N. Rosenbluth, A.H. Teller, E. Teller, Simulations of Liquids and Solids, North-Holland, New York, 1987.
[61] G.B. Deacon, B. Görtler, P.C. Junk, E. Lork, R. Mews, J. Petersen, B. Zemva, J. Chem. Soc. Dalton Trans. 22 (1998) 3887.
[62] P. Atkins, Physical Chemistry, 6th ed., Freeman, New York, 1997.
[63] A.K. Rappe, W.A. Goddard, J. Phys. Chem. 95 (1991) 3358.
[64] G.H. Grant, W.G. Richards, Computational Chemistry, Oxford Science, New York, 1996.
[65] J.E. Carpenter, F. Weinhold, J. Mol. Struct. Theochem. 169 (1988) 41.
[66] R.F.W. Bader, Atoms in Molecules—A Quantum Theory, Oxford Press, New York, 1990.